

UC Davis

UC Davis Previously Published Works

Title

Digital droplet infusion

Permalink

<https://escholarship.org/uc/item/2787q0t0>

Journal

Lab on a Chip, 21(3)

ISSN

1473-0197

Authors

Fang, Zecong

Li, Andrew I

Liu, Hong

et al.

Publication Date

2021-02-07

DOI

10.1039/d0lc00896f

Peer reviewed



Digital droplet infusion†

Cite this: DOI: 10.1039/d0lc00896f

 Zecong Fang, ^a Andrew I. Li,^b Hong Liu^c and Tingrui Pan ^{*,a}

Infusion pumps have been widely used in clinical settings for the administration of medications and fluids. We present the digital droplet infusion (DDI) device, a low-cost, high-precision digital infusion system, utilizing a microfluidic discretization unit to convert continuous flow into precisely delivered droplet aliquots and a valving unit to control the duration and frequency of flow discretization. The DDI device relies on a distinct capillarity-dominated process of coalescence and pinch-off of droplets for flow digitization, which is monitored by a pair of conductive electrodes located before and after the junction. The digital feedback-controlled flow rate can be employed to adjust a solenoid valve for refined infusion management. With this unique digital microfluidic approach, the DDI technology enables a simple yet powerful infusion system with an ultrahigh resolution of digital droplet transfer volume, as small as 57 nL, which is three orders of magnitude lower than that of clinical standard infusion pumps, as well as a wide range of digitally adjustable infusion rates ranging from 0.1 mL h⁻¹ to 10 mL h⁻¹, in addition to an array of programmable infusion profiles and safety features. Its modular design enables fast assembly using only off-the-shelf and 3D-printed components. Overall, benefiting from its simple device architecture and excellent infusion performance, the DDI technology has great potential to become the next-generation clinical standard for drug delivery with its high precision and ultimate portability at a low cost.

 Received 7th September 2020,
 Accepted 27th October 2020

DOI: 10.1039/d0lc00896f

rsc.li/loc

Introduction

Using infusion pumps to deliver medications intravenously has been widely practiced in clinical settings for treating patients that are not responsive to other drug delivery routes such as oral administration.¹ Infusion drug delivery has a long history of nearly 200 years, dating back to the early 19th century when Dr. Thomas Latta had successfully infused a saline solution into patients to provide life-saving rehydration during the deadly cholera epidemic.^{2,3} The modern infusion system is commonly utilized in clinical scenarios, such as chemotherapy, surgery, and pain management, and has been used in the delivery of various medications and supplements including antibiotics, analgesia, anesthesia, and alimentation. It can be administered through intravenous, subcutaneous, epidural, or intrathecal routes. Automated infusion pumps are frequently used, and they have proven to be beneficial in patient care due to their delivery control, precision, and safety compared to manual administration.¹ Infusion pumps vary by

type, and these include external pumps and implanted pumps, ambulatory (portable) and stationary pumps, microinfusion pumps and macroinfusion pumps, *etc.* Microinfusion pumps function to provide accurate and precise infusion of fluids and medications at an infusion rate typically smaller than 10 mL h⁻¹, commonly found in treating pediatric patients or neonates and for administering short-acting or highly concentrated drugs such as vasoactive drugs and inotropic agents.^{1,4,5} Notably, microinfusion pumps remain a critical category of infusion pumps that have drawn more attention recently, owing to the growing demand for precision healthcare and device portability. Typical uses of this type of infusion pump include postoperative pain management (*e.g.*, chemotherapy for cancer patients), chronic disease management (*e.g.*, insulin therapy for diabetic patients), enteral feeding, *etc.*¹ There are currently three types of microinfusion pumps, as shown in Table 1.

The first category, representing disposable mechanical infusion pumps, is considered to have three distinctive subtypes, that is, elastomeric, spring-loaded and vacuum-driven pumps.⁶ These types of mechanical pumps, instead of using electronic driving force, exploit intrinsic mechanical power, such as a stretched elastic membrane, a compressed spring, or the pressure difference across a vacuum chamber, to drive medications. To refine the infusion rates, an adjustable control unit is installed in line with the pump, allowing one to manually switch different flow resistances of the infusion line. On the one hand, disposable pumps are

^a Micro-Nano Innovations (MiNI) Laboratory, Department of Biomedical Engineering, University of California, Davis, CA, 95616, USA.
 E-mail: tingrui@ucdavis.edu

^b Department of Surgery, Division of Plastic Surgery, Hand, Upper Extremity and Microsurgery, University of California Davis Health, Sacramento, CA, 95817, USA

^c Department of Anesthesiology and Pain Medicine, University of California Davis Health, Sacramento, CA, 95817, USA

† Electronic supplementary information (ESI) available. See DOI: 10.1039/d0lc00896f

Table 1 Comparison of the DDI system with available microinfusion pumps

	Mechanical pump	Peristaltic pump	Syringe pump	Digital droplet infusion
Source of driving force	Stretched elastomer, compressed spring, or pressure difference across two sides of a vacuum chamber	Rotating rollers or linear fingers	Linear movement of a stepper motor	Any source that generates a positive pressure
Resolution	Low	Medium	High	High
Accuracy	Low	Medium	High	High
Volume limitation	No	No	Yes	No
Flow stability	Good	Poor	Fair	Good
Response time	Short	Long	Medium	Short
Bolus injection control	Poor	Fair	Good	Good
Program complex infusion profile	No	Yes	Yes	Yes
Flow rate monitoring	No	No	No	Yes
Closed-loop control	No	No	No	Yes
Cost	Low	Medium	High	Low
Representative products	ON-Q* pain relief system, Ambu® ACTion™ block pain pump, Springfusor® syringe infusion pump, COOPDECH Syrinjector.	CADD®-Solis infusion system, CURLIN® ambulatory infusion pump, EnteralLite infinity pump.	MiniMed 670G insulin pump system.	N/A.

cost-efficient and lightweight, possibly due to their simple and purely mechanical design. On the other hand, the actual infusion rates can significantly deviate from the presets, leading to accumulated inaccuracies over 40%, due to the lack of flow rate monitoring and feedback. Multiple factors can contribute to the substantial errors, including the viscosity variations in the drug formula, the pressure variations in the pump, and the imprecise alignment of the flow controllers.⁶ Moreover, the purely mechanical nature of these devices makes the addition of safety features difficult to incorporate, such as alarms for device malfunction or the ability of the device to record an infusion history. This makes it difficult for healthcare workers to check the device if a possible medication delivery error needs to be investigated.⁶

The second category of microinfusion pumps is peristaltic pumps, which are the most widely used electronic infusion pumps currently.¹ The pump functions through rotating rollers or linear actuators to squeeze an elastic tube in a consecutive order, which then pushes a sequence of boluses of infusion fluid from the tube into the patient in a semi-digital manner. The peristaltic pumps are considered more accurate than mechanical pumps, and they also have various safety and alarm features. However, the mode of delivery in peristaltic pumps is inherently intermittent, particularly when working at low infusion rates, and they are limited by their working principle of generating only relatively large volume aliquots. As an example, the CADD Solis pump (Smiths Medical, Inc.), one of the most popular models, has a stroke pumping volume as large as 50 μL .⁷

The third category of syringe pumps is more commonly used to administer medications at extremely low flow rates, which utilize a precision linear movement driven by a stepper

motor to push medications stored in a syringe into the infusion line.¹ Although the syringe pump has the highest reported accuracy and resolution of the three, these pumps experience technical issues, such as start-up delay, displacement position dependent delivery volumes (*e.g.*, vertical placement), and patient back pressure dependent delivery volumes, which can cause appreciable deviations from the preset delivery rate.⁸ Furthermore, the syringe pumps have a loading capacity limited by the size of the syringe and are generally high-cost. Another drawback of these pumps is that they are significantly heavier than the mechanical counterparts, making them less popular for ambulatory or bedside use.⁶

Recently, there has been growing interest in making microinfusion pumps that are capable to infuse at low flow rates with high precision and accuracy, while remaining portable and cost effective.⁸

Microfluidics offers a solution to address this challenge, with its promise for high-precision fluid handling and manipulation at the microscale.^{9,10} Surprisingly, the decades of progress in microfluidic pumps have marginally benefitted the advances of the microinfusion pumps. The majority of the novel micropumps have been intended to be implantable or used for insulin pumps instead of being used for daily infusion drug delivery.^{9,10} For instance, an implantable drug delivery system for pain management (Prometra®, Flowonix Medical) has utilized a conventional diaphragm pump structure for precision microinfusion¹¹ in which a chamber with a capacity of 2 μL has been repeatedly filled and drained, thereby enabling drug dispensing in a digital manner. Another example is an insulin pump design from Tandem Diabetes Care, in which a mobile component slides

between an insulin reservoir and the infusion line, allowing a minimum bolus infusion of 100 nL. Such micropump designs have been proven to be more accurate than the conventional syringe pumps, as they infuse at a definitive volume of liquid in each pumping cycle, in addition to their compact structural design. However, such infusion systems are typically complicated in design and heavily rely on expensive precision machining to be built. Recently, Weiss and colleagues introduced a simplified microinfusion pump design that uses a regular syringe as a drug reservoir that is loaded by a mechanical spring.¹² An external pinch valve is incorporated along with an inline flow sensor to form a closed loop control of the flow to the infusion line.¹² This new type of infusion pump has been shown to be accurate at ultralow flow rates, and now no longer suffers from issues common to standard syringe pumps such as start-up delays and flow irregularities involving hydrostatic changes. Particularly, the inclusion of the flow sensor enables the precise quantification of the infused liquid;¹³ however, this sensor, a high-precision microflow metering unit, also substantially increases the cost of the system.¹⁴ Though holding great potential in manipulating fluids with high precision, microfluidic technologies have not yet been fully exploited for practical uses in low-cost and daily microinfusion therapies.

Recently, a novel high-precision flowmetry concept, known as digital droplet flowmetry, has been proposed by our group, utilizing interfacial instability to discretize continuous flow into uniform units of droplets.^{14–16} Such a digital flowmetry technology has achieved a high resolution of 2.5 nL with a simple detection scheme, and its low-cost assembly can be used for disposable applications.¹⁴ In this study, we have incorporated this droplet flowmetry design in the proposed infusion system, enabling its high-precision flow measurements and instantaneous feedback to flow control. As such, the proposed digital droplet infusion (DDI) system employs droplet flowmetry to convert a continuous microflow into countable transfer volumes for analog-to-digital flow measurement; meanwhile the detected flow rates are feedbacked to adjust the upstream valving unit for the desired stable infusion. Benefiting from its modular design, the DDI device can be assembled using only off-the-shelf and 3D-printed components, while achieving a wide range of clinically viable microinfusion rates covering 0.1 mL h^{-1} to 10 mL h^{-1} , with a precision resolution of single droplet transfer volume down to 57 nL, three orders of magnitude smaller than the commonly used clinical portable infusion pumps (CADD Solis, Smiths Medical Inc.). Notably, the prior art has demonstrated the concept of digital droplet flowmetry on chip, while in this work, we have incorporated a digital droplet flowmetry unit into a closed-loop control system with a pressure source, leading to an independently-operating high-precision pumping device, which has outperformed the existing pumps as characterized in the following categories. A comparison between the DDI system and the available microinfusion pumps can be found in Table 1. To

demonstrate the utility of DDI for infusion drug delivery, various infusion profiles have been successfully generated by programming the opening and closure of the electronic valve unit with the feedbacked flow rate measurements. In addition, various key safety features have been demonstrated, including the real-time monitoring of the infusion dosage and the detection of occlusion, for clinical considerations.

Operating principles

As aforementioned, the proposed DDI system has utilized the droplet flow discretization concept^{14–16} for digital flow measurement and the detected flow rate is then feedbacked to the upstream for flow control by an electronically driven valve. As depicted in Fig. 1a, the DDI device is mainly composed of three modular components, namely the flow discretization unit, a valving unit, and an electronic control unit. The inlet of the DDI device is connected to a high-pressure source, either an elastomeric pump or a hydrostatic pressure source. The valving unit controls the liquid flow from the high-pressure source with single-digit millisecond resolution. The flow discretization unit then turns the continuous flow into uniform and countable droplets with high precision. Subsequently, the electronic control unit

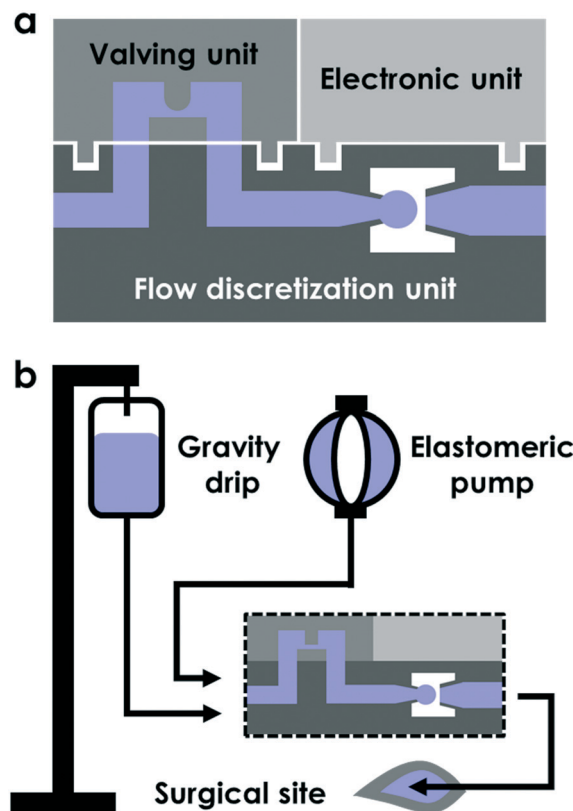


Fig. 1 Concept of the digital droplet infusion (DDI) system. a) Illustration of the concept of DDI, including a flow discretization unit, a valving unit, and an electronic control unit; b) illustration of the practical use of a DDI device, which can be attached to either a standard elastomeric pump or a gravity-based administration set.

detects the impedance variation in the flow discretization unit to monitor and calibrate the amount of liquid that has been transferred. In order to achieve the desired preset value, the measured flow rate is feedbacked to adjust the valve accordingly as a closed-loop control. In addition, simple programming of infusion profiles can be implemented with fine temporal tuning of valving settings. As illustrated in Fig. 1b, the DDI device can be conveniently integrated in-line into a conventional elastomeric pump or a gravity-based intravenous infusion set for high-precision digital infusion drug delivery. The DDI device can be turned into a lightweight design with a small footprint. Benefiting from such a modular design, all the electronic and fluidic components of the DDI device are independently operated, enabling the low-cost disposable design of the self-contained fluidic unit.

Fig. 2a illustrates the dynamic process of flow discretization with the capillarity-governed droplet coalescence and pinch-off events illustrated, similar to that previously reported.¹⁴ In brief, the initial droplet has a volume of V_r , and increases gradually to a volume of V_c and a radius of R_c under the flow when coalescing with the downstream collecting interface. The droplet emergence process takes a total duration of t_e . Once the droplet comes into contact with the droplet-collecting interface, a liquid bridge forms and then autonomously snaps off under the dominance of capillary forces over inertia, transferring a volume of V_t to the downstream. After the pinch-off, a droplet volume of V_r remains, and the cycle repeats itself. The process of liquid bridging takes another duration of t_b .

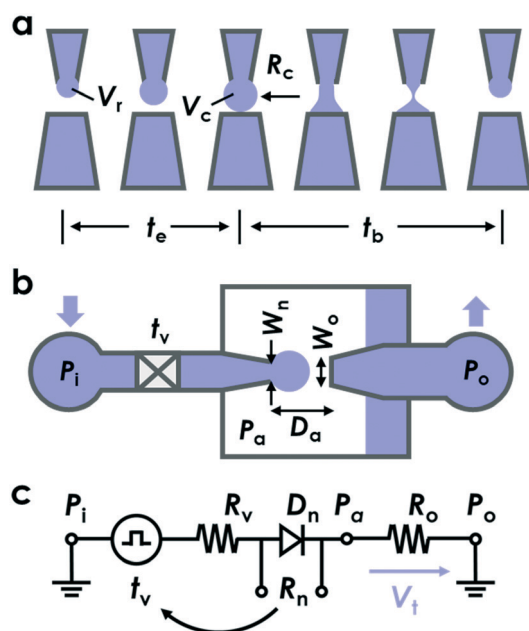


Fig. 2 Working principle of the digital droplet infusion (DDI) system. a) Illustration of the process of droplet emerging, coalescing, and pinching off under the pulsed driving pressure; b) cross-sectional illustration of the DDI device, with governing parameters for the flow discretization unit and valving unit labeled; c) analogical hydraulic circuit modeling of DDI.

Furthermore, the governing parameters for the DDI device have been identified and labeled in Fig. 2b. In the flow discretization unit, a microscale orifice with a diameter of W_n is intruded into a sealed air-buffered chamber for droplet generation. On the opposing side, another orifice with an opening diameter of W_o is included to collect the droplets at a separation distance of D_a and transfer them to the downstream. It is worth noting that the tapered shape at the collection site facilitates automatic priming, in order to minimize the total surface energy at the tip.¹⁷ At a low flow rate, the process for droplet formation and removal is dominated by capillarity, with the flow inertia largely neglected.¹⁴ In this scenario, the droplet transfer volume (V_t) becomes a liquid-specific and geometrically-determined (R_c) constant that can be decoupled from the incoming flow rates, according to our previous investigation.¹⁴ It is mainly dictated by the nozzle size W_n and separation distance D_a , while the opening of the droplet-collecting site W_o has less influence. Meanwhile, the liquid in the flow discretization unit seals a small volume of air with a buffered air-liquid interface. As the outlet pressure (P_o) rises up, the buffering interface moves towards the nozzle and compresses the air inside the chamber to increase the chamber pressure (P_a) accordingly, reaching approximately $P_a \approx P_o$ under quasi-static states and thus balancing the variations in the outlet pressure. Upstream of the DDI, an electronically controlled valve is used to adjust the duration of the starting and stopping of the flow from the input pressure source (P_i), with an opening time of t_v .

An equivalent hydraulic circuit of the DDI device is drawn in Fig. 2c to further clarify the working principle. Notably, variation of the impedance (R_n) across the nozzle can be used not only to count the number of droplets but also to self-calibrate the transferred liquid volume. In addition, the computed flow rates from the counted droplet number and the transfer volume are maneuvered as a feedback signal to the valve unit for fine tuning of the valve opening time. It is worth noting that the droplet transfer volume (V_t) is a liquid-specific and geometrically-determined (R_c) constant, as thoroughly analyzed in the previous study.¹⁴ The droplet transfer volume can be calibrated, for instance, it is experimentally determined to be 57 nL for a 312 μm nozzle and 673 nL for a 718 μm nozzle using the saline solution in this study, as demonstrated in section ‘‘Parametric analysis of the DDI devices’’. The relevant flow resistances in the upstream (R_v) and downstream (R_o) of the nozzle are also labeled in Fig. 2c, respectively, both of which could influence the responsiveness of the DDI device. Specifically, during the working of DDI, the valving duration (t_v) will be fixed and the delay (t_{delay}) between the consecutive valve openings can be tuned to generate a range of valving frequencies as $f_v = 1/(t_v + t_{\text{delay}})$, and produce various averaged infusion rates as $Q_{\text{avg}} = f_v \cdot Q \cdot t_v$. Since t_v will be fixed and t_{delay} is adjustable, shortening the valving duration would lead to a higher valving frequency with more adjustability and control. Here Q is the flow rate of DDI during the valve opening duration,

which correlates with the pressures and flow resistances as $Q = (P_i - P_o)/(R_v + R_n + R_o)$. By substituting the formulas of f_v and Q , we have $Q_{\text{avg}} = t_v/(t_v + t_{\text{delay}}) \cdot (P_i - P_o)/(R_v + R_n + R_o)$. On the other hand, by discretizing the continuous flow into uniform droplets, the averaged infusion rate correlates with the droplet transfer volume as $Q_{\text{avg}} \approx f_v \cdot N \cdot V_t$. Here N denotes the number of droplets transferred within each duration of valve opening when $t_v > t_e$, since if $t_v < t_e$ (droplet emerging duration) no droplet or single droplet transfer would occur, *i.e.*, $N \leq 1$. As a result, the averaged infusion rate Q_{avg} can be conveniently adjusted by tuning the delay t_{delay} between the consecutive valve openings, while it can also be monitored by multiplying the number of droplets transferred (N) during each event of valve opening and the corresponding valving frequency (f_v).

Materials and methods

The fabrication of the DDI devices is straightforward and the assembly process can be done rapidly. As shown in Fig. 3, a translucent manifold was 3D printed as the interface for the valving unit and the flow discretization unit, by outsourcing from a prototyping company (Fictiv). The 3D prints are made of two pieces that can be reversibly assembled with designed thread structures. The first piece has two straight holes designed to attach and seal the solenoid valve (Lee Company LHD series) that has single-digit millisecond temporal resolution. In addition, the first piece has two 90 degree elbow channels, one connecting the valve to the inlet of the DDI device and the other connects to the downstream flow discretization part, respectively. The flow discretization part has a Luer-slip structure designed to attach a stainless-steel

needle (size from 22G to 33G, Nordson EFD and Hamilton Company) for droplet generation, which is in blue color as shown in the image. The second piece of the 3D prints has a taper-shaped structure for automatic priming and droplet removal as aforementioned, and it can be screwed into the first piece for reversible sealing, with Teflon tapes applied to enhance airtightness. Once the two 3D printed pieces were assembled, they were aligned coaxially, and the separation distance was finely adjusted by tuning the threads. In cases where a 3D printer is not available, the DDI device could also be made *via* a low-cost and completely off-the-shelf scheme, as shown in Fig. S1.† Briefly, an off-the-shelf stainless-steel needle was used for droplet generation, and a plastic tapered dispensing tip (20G, Nordson EFD) was used for the removal of the droplets. Both the stainless-steel needle and the plastic dispensing tip were inserted into a clear acrylic plastic tube (1/4" OD, 1/8" ID), carefully aligned and sealed at both ends with hot glue to form an airtight chamber. The plastic tube was precisely cut using a CO₂ laser (VersaLaser, Universal Laser System). It is worth noting that two 2 mm holes were drilled in the middle of the plastic dispensing tip, which allowed the liquid to flow gradually back into the air-buffered chamber to compensate for the variations of back pressure, as mentioned previously. In addition, two electrodes were inserted and sealed into the connecting portion of the stainless-steel needle and the plastic dispensing tip, respectively. The solenoid valve was connected with the flow discretization unit *via* a needle and a Luer-slip adapter (Cole-Parmer), and the connection junctions were carefully sealed with hot glue.

To test the performance of the DDI devices, 0.9 wt% saline was used as the working fluid. The inlet of DDI was connected to a pressure pump (PeciGenome) and its outlet was connected to a beaker to collect the drainage liquid, *via* plastic tubing. A miniature PEEK tube (125 μm in OD and 10 cm in length, IDEX) was added to the tubing between the pressure pump and the DDI device to restrict the range of the flow resistance and the resultant flow rate range. The inlet pressure of the DDI device was adjusted by finely adjusting the output pressure of the pump, while the outlet pressure of the DDI device was adjusted by changing the height of the distal end of the plastic tubing to reach a range of desired testing hydrostatic pressures. To quantify the unit droplet transfer volume, a gravimetric method was used, in which a balance (Mettler Toledo AB54-S/FACT) with a high resolution of 0.1 mg was used to weigh the collected liquid from the distal end. The opening duration and frequency of the solenoid valve were conveniently adjusted using an open-source microcontroller (Arduino Mega 2560) and custom algorithms. To detect the impedance change and monitor each of the coalescence and pinch-off events, a simple electrical circuitry driven by a DC power supply (BNC Model 1533) and a function generator (BNC Model 645) was used, similar to the one reported in our previous work.¹⁴ The output impedance signal was acquired by a DAQ board (National Instruments, USB-6210) at sampling rates of 1 and

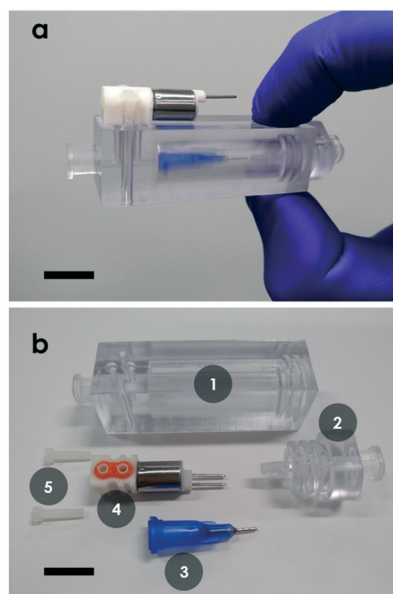


Fig. 3 Prototype of the DDI device. a) Assembled DDI device; b) key components in DDI, including 1 – first piece of 3D prints, 2 – second piece of 3D prints, 3 – stainless steel needle, 4 – solenoid valve, and 5 – fastening screws for the valve. The scale bars are 1 cm.

10 kS s⁻¹ and displayed with a LabVIEW interface. It is worth noting that two electrodes were integrated into the DDI device, and to avoid any potential contamination or electrochemical reaction, an ultralow AC electrical voltage with a magnitude of 1 mV can be applied to assess the events of droplet coalescence and pinch-off electrically.¹⁸ In addition, both inert electrode materials and corrosion-resistant coatings can be considered to reduce the risk of electrochemical contamination in future.¹⁹ Furthermore, a high-speed camera (Phantom VEO-E 310 L) was connected with a microscope (Omano) to record the shape evolution of the droplet dynamics in the process of emergency, coalescence and pinch-off, at a frame rate of 10 000 fps.

Results and discussion

Following the operating principles of the DDI device, we first investigated the dynamics of valve-controlled flow discretization (VCFD) and the influence of valving duration on the droplet transfer volume. Second, we conducted a parametric study to evaluate the various governing parameters in the DDI system, including the geometry of the flow discretization unit, the input pressure, and the back pressure. After the characterization of the system, we demonstrated the use of DDI for the convenient programming and generation of five commonly used infusion profiles, in addition to the real-time monitoring of infusion

dosage and the sensitive detection of occlusion in the infusion line.

Dynamics of the valve-controlled flow discretization (VCFD)

The dynamic process of droplet emergence, coalescence and pinch-off in a DDI device was recorded with a high-speed camera and some of the snapshots in one cycle are shown in Fig. 4a. In this particular nozzle configuration in this study, the droplet was stably pinned at the outer edge of the needle, due to the structural confinement (also known as the canthotaxis effect),²⁰ throughout the dynamics of coalescence and pinch-off. Moreover, the droplet was in a spherical cap shape (undistorted) during the emerging phase, as can be seen in Fig. 4a, since the device was primarily working under low-flow rate conditions within the capillary limit.¹⁷ In brief, according to our experimental observation and the canthotaxis effect, the surface chemistry would not apparently affect the dynamics of coalescence and pinch-off due to droplet pinning. However, for certain low surface tension liquids, for instance ethanol, its contact line might move beyond the edge of the needle; thus, further hydrophobic treatment on the outer wall of the needle becomes necessary to immobilize the contact line at the edge.

The DDI device used has a nozzle width W_n of 718 μm and a separation distance to nozzle width ratio (D_a/W_n) of

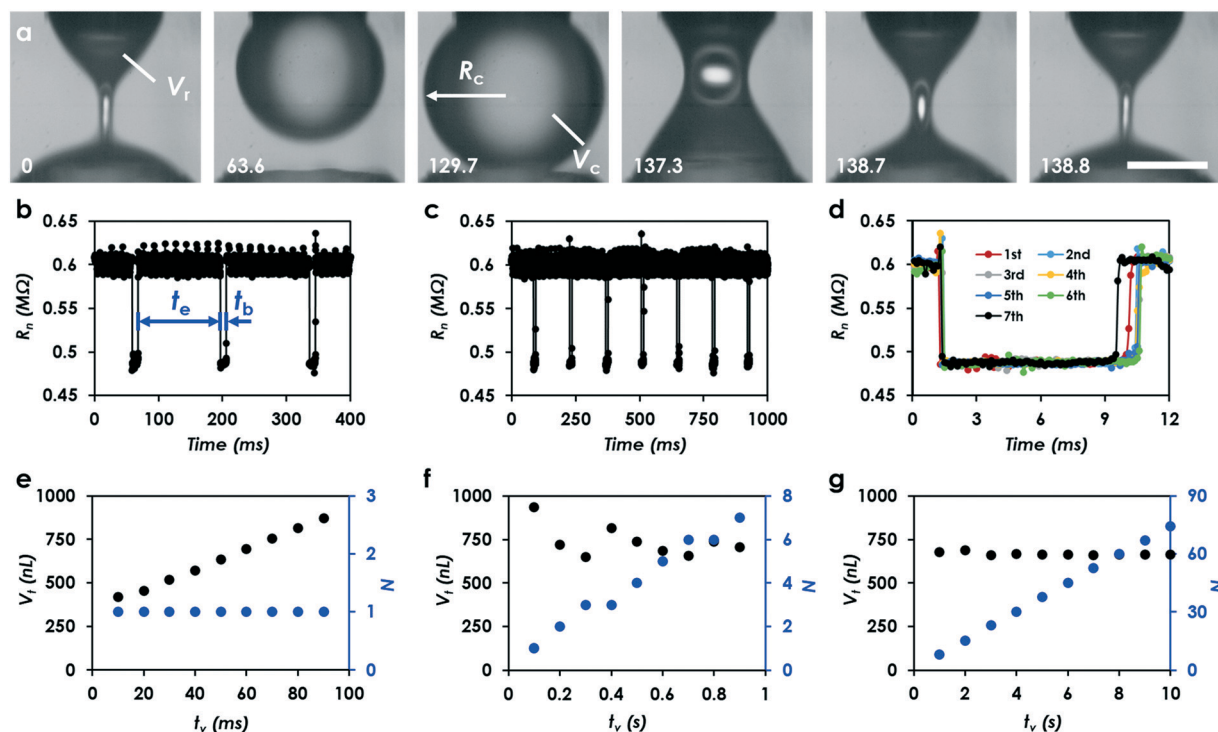


Fig. 4 Dynamics of the valve-controlled flow discretization (VCFD) process in the DDI system. a) High-speed images of the coalescence and pinch-off events during the flow discretization with the valve fully open, the listed times are in milliseconds and the scale bar in the last frame is 500 μm ; b) electrical measurement of the flow discretization with the valve fully open; c) electrical measurement with a transient valving opening duration of 1 s; d) the zoom-in view of the impedance change during the liquid bridging status; e–g) the droplet transfer volume and the number of droplets transferred at various valving durations.

1.25, the input pressure was set at 10 psi, and the valve was kept open all the time. The duration of emerging t_e was found to be 129.7 ms, and the duration of liquid bridging t_b was 9.1 ms. Since the flow resistance was high and the flow rate was low, the droplet maintained a spherical cap shape during the process of emerging and it was not otherwise distorted, as expected. During the liquid bridging process, a liquid meniscus formed, as highlighted in the snapshot at 137.3 ms (Fig. 4a), which eventually snapped off due to the dominance of capillarity over inertial force. As aforementioned in the section of Operating principles, when the flow rate is low (Weber number $We \ll 1$), the droplet transfer volume can be approximated as $V_t \approx V_c - V_r$, becoming a liquid-specific and geometrically determined constant as evidenced later in the following discussion.¹⁴ Moreover, the impedance across the DDI junction, R_n , fluctuated as the flow discretization occurred periodically at the nozzle during the phase of valve opening, as shown in Fig. 4b. Consecutively, the events of droplet coalescence and liquid bridge pinch-off were successfully detected. In particular, the impedance was 0.60 M Ω during droplet emergence and then dramatically dropped to 0.48 M Ω during the liquid bridging phase. The duration of liquid bridging t_b of 9.1 ms can be measured from the electrical signal, the same as the results from the optical high-speed imaging. On the other hand, the duration of droplet emerging t_e of 129.4 ms can also be deduced from the electrical signals and is also in agreement with the imaging results. In brief, each duration of the repetitive bridging and emerging processes lasted 138.5 ms. It is worth noting that the electrically measured emerging time of 129.4 ms was the average of 5 consecutive measurements, and the standard deviation between the measurements was 0.7 ms. The optically measured emerging time of 129.7 ms was recorded once, leading to a duration of 0.3 ms longer than the electrical measurement, but it is still within the permitted tolerance of the measurements.

In the next step, we investigated the electrical signals during a VCFD process. Fig. 4c shows the recorded electrical measurement of a flow discretization event when the valve temporarily opened for 1 s in the same DDI device. Seven events of droplet coalescence were successfully detected, in which the droplets had an average temporal spacing of 139.3 ms, which was consistent with the aforementioned flow discretization scenario when the valve remained open. As further clarified in Fig. 4d, the impedance profiles of the seven droplets closely overlapped with each other during the liquid bridging states, with an averaged t_b of 9.0 ms and standard deviation of 4.1%. The outlying first droplet had a shorter bridging duration of 8.9 ms and the outlying last droplet had a bridging duration of 8.2 ms, most likely due to the sudden acceleration of the flow at the instant that the valve opened or closed.

To further elaborate the effects of valving duration (t_v) on the droplet transfer volume, a thorough study covering three orders of magnitude in the valving duration (from 10 ms to

10 s) was conducted, as exemplified in Fig. 4e–g, using the same DDI device. In addition, the number of droplets transferred (N) in each of the preset durations of valving was also reported. As mentioned in the section of Operating principles, shortening the valving duration leads to a higher controllable and adjustable valving frequency, hence here we intend to find the shortest valving duration that is suitable for the targeted infusion pumping, so that we can have more flexible control of the infusion rate. 10 ms was chosen as the lower limit since the response time of the solenoid valve used was 5 ms, therefore one cycle of opening and closure of the valve was in total 10 ms; shorter than 10 ms would lead to abnormal working conditions of the valve. As shown in Fig. 4e, when the valving duration was increased from 10 ms to 90 ms, the droplet transfer volume linearly increased from 417 nL to 870 nL, accordingly. For valving duration from 10 ms to 90 ms, only a single droplet was transferred to the downstream each time the valve opened, of which the volume was proportional to the time of valve opening.²¹ It is worth mentioning that during such a droplet transfer regime (t_v from 10 ms to 90 ms), the droplet transfer volume could be conveniently adjusted by tuning the valving duration; however, it is also influenced by the input pressure.²¹ Briefly, a higher input pressure results in a higher flow rate, and thus the droplet transfer volume would increase accordingly. Therefore, this regime may not be best suitable for infusion pumping applications, due to this input pressure dependence. Furthermore, the results of flow discretization with a longer valving duration from 0.1 s to 0.9 s are depicted in Fig. 4f. As can be seen, the averaged droplet transfer volume is close to each other but not consistent within the studied valving durations. In particular, the droplet transfer volume is averaged at 739 nL within the t_v range from 0.1 s to 0.9 s and has a standard deviation of 12.1%. As evidenced in Fig. 4d, the inconsistency of the transfer volume can be largely attributed to the abnormality of the first and last outlying droplets during each valve opening event, which became appreciable due to the small number of droplets formed during each valve opening. As we kept increasing the valving duration to 3 s or above, as shown in Fig. 4g, the number of droplets in each valving increased to 23 and above, and the droplet transfer volume was found to be highly constant at 664 nL from 3 s to 10 s, with a standard deviation less than 1%. It is worth noting that a standard deviation of less than 3% was used as a criterion to determine the threshold stable valving duration in the current study. Notably, the nominal accuracy of a commercially available electrical pump (CADD Solis, Smiths Medical Inc.) is listed as 6%; we have chosen an accuracy of 3% to reflect its higher accuracy than that of the commercial counterpart, while reaching a considerably higher resolution and precision (57 nL) under the simple pumping architecture. According to this criterion, the threshold valving duration for a 515 μm nozzle was measured to be 1 s and that for a 312 μm nozzle was 0.7 s, with the ratio of separation distance and nozzle width D_a/W_n fixed at 1.25, the

same as the 718 μm nozzle. In such cases, the dispersion became negligible, indicating that the influence of the valve transient states was no longer appreciable on the droplet transfer volume. It also manifested a new regime that was capillarity-governed, where the inertial force had a negligible effect, and thus, working under such a regime was suitable for infusion pumping. Within such a regime, the VCFD process behaved similar to the one under a continuous flow.^{14,16} Therefore, a threshold valving duration that corresponds to a deviation smaller than 3% was experimentally determined, and it was chosen as the optimal setting governed by capillarity to control the flow digitalization process with high accuracy and high repeatability, under which the droplet transfer volumes stayed consistent with only a marginal variation.

Parametric analysis of the DDI devices

As aforementioned, to achieve flexible and programmable microinfusion, we proposed a valving frequency control mode, in which the valving duration (t_v) is fixed and the delay (t_{delay}) between consecutive valving and frequency of valve opening (f_v) can be exerted to adjust the averaged liquid infusion rate (Q_{avg}). In such a working mode, an ultra-low while clinically meaningful infusion rate at the scale of 0.1 mL h^{-1} can be produced since the valving frequency can be preset to be extremely low. Since the fastest acting drug in an intensive care unit (ICU) has a half-time of 150 s, of which the inverse determines the minimal acceptable infusion frequency, namely 1/150 Hz.²² In this study, we have set 0.01 Hz as our minimal infusion frequency threshold accordingly. In addition, reducing the separation distance while having the nozzle width fixed leads to a higher resolution of droplet transfer; however, it is prone to form a stable liquid bridging that could not be pinched off, leading to the termination of the flow discretization process.¹⁴ A ratio of separation distance and nozzle width D_a/W_n of 1.25 has been previously reported as an optimal ratio for generating high resolution droplet transfer under capillarity-induced digitalization.¹⁴ We therefore have adopted our geometrical ratio of 1.25 for all the DDI devices under this investigation. Fig. 5a presents the experimental results of DDI devices with three different nozzle widths that work at various valving frequencies,

validating the fine control of the infusion rate by tuning the valving frequency. For a DDI device with a W_n of 718 μm , the valve opening duration was fixed at 3 s for stable infusion to eliminate the effects of the outlying droplets as aforementioned. The valving frequency was increased from 0.01 Hz to 0.19 Hz to generate the resultant averaged infusion rate from 0.51 to 10 mL h^{-1} . The mean droplet transfer volume was 673 nL. As can be seen, the infusion rate was proportional to the infusion frequency, with the slope corresponding to a transferred volume of 14.5 μL , which was the liquid transferred during the 3 s of valve opening duration. The 515 μm device had a droplet transfer volume of 250 nL, and its valving frequency of 0.01 Hz resulted in a minimal infusion rate of 0.17 mL h^{-1} on average and the targeted infusion rate of 10 mL h^{-1} was reached at a valving frequency of 0.53 Hz. As indicated in Fig. 5a, for the 312 μm DDI device, the valving frequency was increased from 0.01 to 0.77 Hz, and the resultant infusion rates covered our targeted infusion rate range, from 0.1 to 10 mL h^{-1} . Reducing the nozzle width to 312 μm helped lower the droplet transfer volume to 57 nL, which is three orders of magnitude smaller than the commonly used portable infusion pumps (CADD Solis, Smiths Medical Inc.) in clinical settings. Similarly, the slope of the plot corresponded to the total liquid transferred during the valve opening duration, which was found to be 3.3 μL on average. We further reduced the nozzle size to 210 μm but found that the linear range of droplet transfer volume was smaller than our targeted flow rate of 10 mL h^{-1} , and therefore it was not suitable for typical drug infusion applications.¹ On the other hand, increasing the nozzle size to be greater than 718 μm is not suitable for clinical applications, since the valving frequency would need to be smaller than our preset minimum of 0.01 Hz to reach the targeted minimal infusion rate of 0.1 mL h^{-1} .

Influences of input pressure and back pressure

For the practical use of DDI in clinical settings, we had also studied the effects of the variations of pressure in the pump and at the patient site (back pressure). As presented in Fig. 5b, the input pressure was set from 4 psi to 11 psi for a DDI device with a 515 μm nozzle width, matching the pressure range commonly found in disposable infusion

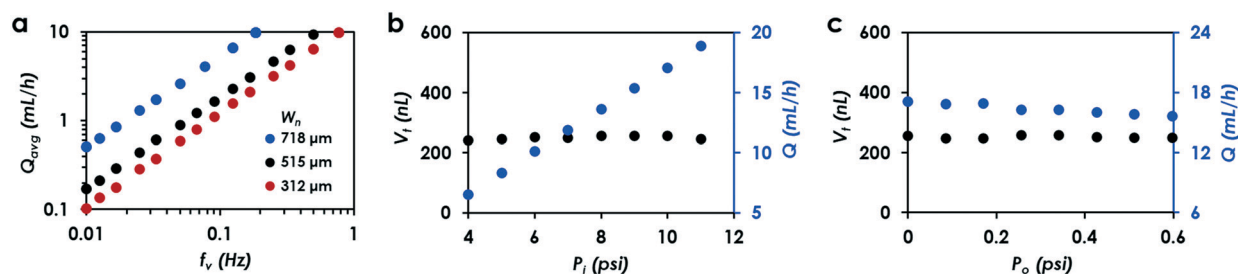


Fig. 5 Characterization of the DDI device. a) Adjustment of the infusion rate at various frequencies of valving, with a fixed ratio of separation distance to nozzle width of 1.25; b) droplet transfer volume and infusion rate under input pressures from 4 to 11 psi for a 515 μm nozzle; c) droplet transfer volume and infusion rate under outlet back pressures from 0 to 0.6 psi for a 515 μm nozzle.

pumps, which is 4.8 to 11.6 psi (250 to 600 mmHg).⁶ The valve was kept open and the droplet transfer volume was measured under various input pressures. As can be seen, the droplet transfer volume was found to be a constant of 250 nL, with a standard deviation of 2.3%, over the broad pressure range investigated. Fig. 5b also shows the plot of the corresponding flow rates at different input pressures, 6.5 mL h⁻¹ at an input pressure of 4 psi, and 18.9 mL h⁻¹ at 11 psi. The increased input pressure would lead to a faster discretization process,^{14,16} which could be instantaneously tracked by the built-in metering electrodes. Thus, as long as the droplet transfer volume stayed unchanged, the pressure influence from the input line could be precisely compensated for by the measured flow rate.

The effects of the outlet pressure were also investigated and plotted in Fig. 5c. The clinical operation required the outlet pressure to be regulated not to exceed 0.58 psi (30 mmHg), above which it could lead to acute compartment syndrome (ACS).²³ Therefore, the outlet pressure was adjusted between 0 and 0.6 psi (31 mmHg) to simulate the pressure variations at the surgical site of a patient. A DDI device with a nozzle width of 515 μm and an input pressure of 10 psi was tested, and the valve was kept open during the testing. As can be seen, the droplet transfer volume was found to be at a constant of 252.2 nL, with a standard deviation of 2.0%, covering the pressure range from 0 to 0.6 psi. The flow rate under each back pressure was also measured and presented in Fig. 5c. The flow rate was recorded at 17.1 mL h⁻¹ initially, and then slightly reduced to 15.6 mL h⁻¹ as the pressure drop across the DDI device lowered as the outlet pressure rose from 0 psi to 0.6 psi. Overall, these results validated that the digitalization process is independent from the input and back pressure, allowing a consistent and accurate performance of the DDI

device, which was of essence for its future use in clinical settings.

Demonstration

To demonstrate the programmability of the DDI device for infusion drug delivery and infusion therapy, several commonly used infusion profiles were digitally programmed and successfully implemented, and both the infusion rates and the delivered dosages were monitored in real-time as shown in Fig. 6, including (a) the patient-controlled analgesia (PCA), (b) continuous, (c) intermittent, (d) step, and (e) tapered infusions. For all the results presented in the demonstration, a DDI device with a nozzle width of 515 μm was used and the input pressure was set at 10 psi. As indicated in Fig. 6a, for the PCA mode, the basal infusion rate was fixed at 3.3 mL h⁻¹, while the infusion rate was increased to the maximum of 16.7 mL h⁻¹ in the bolus mode. The first bolus was at 18 s after the beginning of infusion, and it lasted for 2 min, delivering 561 μL of dosage; the second bolus was at 198 s, and it last for 1 min, delivering 285 μL of another bolus dosage. For the continuous infusion mode shown in Fig. 6b, the basal infusion rate was also set at 3.3 mL h⁻¹, and after 48 s, it was adjusted to be infusing continuously at 9.9 mL h⁻¹, by increasing the frequency of valving. In the intermittent infusion mode shown in Fig. 6c, infusions at 9.4 mL h⁻¹ that last for 1 min were equally spaced by 30 s. For the step-adjusted infusion shown in Fig. 6d, three steps of increment in infusion rates were achieved by steadily increasing the valving frequency, rising infusion rates from 3.2 mL h⁻¹ to 4.7 mL h⁻¹, 6.3 mL h⁻¹, and 9.5 mL h⁻¹, respectively. A tapered ramp-up and ramp-down infusion profile covering the delivery rates from 3.2 mL h⁻¹ to 6.3

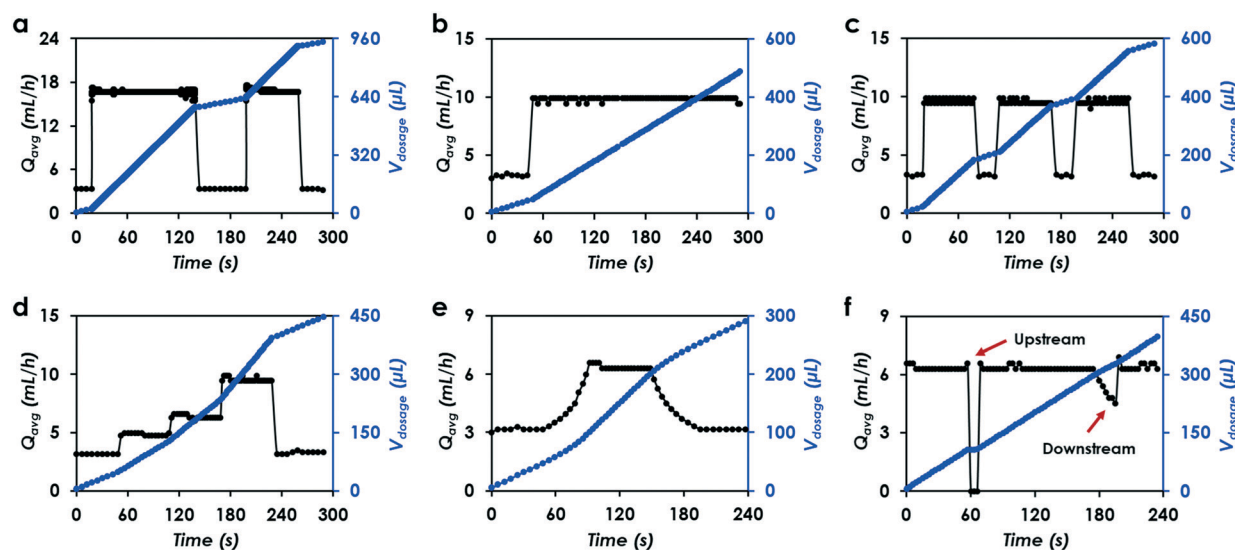


Fig. 6 Demonstration of the DDI system. Real-time infusion rate profile and the volume of dosage at the mode of a) PCA, b) continuous infusion, c) intermittent infusion, d) step infusion, and e) tapered infusion; f) detection of the occlusion at both the upstream and downstream of the DDI device.

mL h⁻¹ was also generated successfully, by gradually adjusting the valving frequency, as can be seen in Fig. 6e.

Lastly, we demonstrated the capability of the DDI device to detect the occlusions in the infusion line. As highlighted in Fig. 6f, the infusion rate was set at 6.3 mL h⁻¹ and the occlusions from both the upstream and the downstream of the DDI device were detected and reflected in the impedance measurement in the DDI device and the corresponding infusion rate readouts. As can be seen, the signals of the upstream and downstream occlusion were obviously distinguishable. Particularly, the blockage of the upstream infusion line resulted in a sudden stop of the input pressure supply and thus the flow rate was decreased to zero. In contrast, the blockage of the downstream infusion line lowered the flow rate but did not stop the flow; it was observed that the liquid started to accumulate in the air-buffered chamber under the continuous flow, as the occlusion increased the flow resistance in the downstream infusion line. In brief, the DDI device not only offers the function of occlusion detection, but also differentiates signals from the upstream and downstream occlusions, and therefore, could enable clinicians to quickly locate the potential issues of the infusion line as an additional safety feature.

Conclusions

In this study, we have presented an innovative low-cost infusion system design, referred to as digital droplet infusion (DDI), for high-precision portable fluid infusion. Based on a distinct capillarity-dominated droplet coalescence and pinch-off process, the DDI device utilizes a flow discretization unit to convert continuous flow into uniform and countable droplets and employs a valving unit that tightly controls the flow discretization events. A theoretical model has been built to elaborate the working principles of the DDI technology and a thorough parametric study has been conducted to investigate the governing parameters that influence the consistency of the unit droplet transfer volume, including the inlet and outlet pressures, the duration and frequency of valving, and the geometric dimensions of the flow discretization unit. Compared with currently available microinfusion systems, the DDI device offers several distinct advantages: 1) high infusion resolution up to 57 nL, three orders of magnitude smaller than the commonly used clinical portable infusion pumps (CADD Solis, Smiths Medical Inc.); 2) wide measurement range from 0.1 mL h⁻¹ up to 10 mL h⁻¹; 3) high accuracy with error less than 3%; 4) direct inline integrability; 5) small footprint and lightweight construction; 6) modular architecture with the electronic and fluidic units operated independently; 7) disposable design of the self-contained fluidic unit with low-cost assembly using off-the-shelf components and 3D-printed parts; 8) programmable digital infusion profiles with both basal and bolus infusion included; 9) multiple safety and alarm features included, such as flow rate setup and adjustment,

calculation of the overall infusion volume, and detection of occlusion, among the others. Benefiting from its simple architecture yet high-performance design at low cost, the DDI technology becomes a promising candidate for the next-generation drug infusion systems.

Conflicts of interest

There are no conflicts to declare.

Acknowledgements

This work was in part supported by 2020 Seed Fund Award 2020-0000000096 from CITRIS and the Banatao Institute at the University of California. ZF would like to acknowledge the fellowship support from Superfund Research Program at UC Davis from the National Institutes of Health (2P42ES004699).

References

- 1 U. R. Kim, R. A. Peterfreund and M. A. Lovich, *Anesth. Analg.*, 2017, **124**, 1493–1505.
- 2 N. MacGillivray, *J. Infect. Prev.*, 2009, **10**, S3–S6.
- 3 J. E. Cosnett, *Lancet*, 1989, **333**, 768–771.
- 4 R. A. Peterfreund and J. H. Philip, *Expert Opin. Drug Delivery*, 2013, **10**, 1095–1108.
- 5 C. M. T. Sherwin, N. J. Medlicott, D. M. Reith and R. S. Broadbent, *Arch. Dis. Child.*, 2014, **99**, 590–594.
- 6 E. A. Skryabina and T. S. Dunn, *Am. J. Health-Syst. Pharm.*, 2006, **63**, 1260–1268.
- 7 CADD@-Solis VIP Ambulatory Infusion Pump Technical Manual, <https://infusystem.com/images/manuals/CADD%20Solis%20VIP.pdf>, (accessed 11 November 2020).
- 8 R. I. Cook, *Can. J. Anaesth.*, 2000, **47**, 929–935.
- 9 F. P. Pons-Faudoa, A. Ballerini, J. Sakamoto and A. Grattoni, *Biomed. Microdevices*, 2019, **21**, 47.
- 10 R. Bisht, A. Mandal and A. K. Mitra, in *Emerging Nanotechnologies for Diagnostics, Drug Delivery and Medical Devices*, Elsevier, 2017, pp. 249–290.
- 11 P. Burke and P. O'Connor, *U.S. Pat.*, No. 8,273,058, 2012.
- 12 M. Batliner, M. Weiss, S. A. Dual, B. Grass, M. Meboldt and M. Schmid Daners, *Anaesthesia*, 2019, **74**, 1425–1431.
- 13 J. Amoores, J. Mather, D. H. T. Scott and K. Craig, *Anaesthesia*, 1998, **53**, 1231–1232.
- 14 Z. Fang, Y. Ding, Z. Zhang, F. Wang, Z. Wang, H. Wang and T. Pan, *Lab Chip*, 2020, **20**, 722–733.
- 15 Y. Yang, S. Xing, Z. Fang, R. Li, H. Koo and T. Pan, *Lab Chip*, 2017, **17**, 926–935.
- 16 X. Li, Y. Mao, Z. Zhu, Y. Zhang, Z. Fang, D. Wu, H. Ding, T. Pan, B. Li and J. Chu, *Microfluid. Nanofluid.*, 2019, **23**, 2–7.
- 17 P.-G. de Gennes, F. Brochard-Wyart and D. Quéré, *Capillarity and Wetting Phenomena*, Springer, 2004.
- 18 J. D. Paulsen, *Phys. Rev. E: Stat., Nonlinear, Soft Matter Phys.*, 2013, **88**, 063010.
- 19 M. Ates, *J. Adhes. Sci. Technol.*, 2016, **30**, 1510–1536.
- 20 J. Berthier and K. A. Brakke, *The Physics of Microdroplets*, John Wiley & Sons, 2012.

- 21 J. Wang, K. Deng, C. Zhou, Z. Fang, C. Meyer, K. U.-A. Deshpande, Z. Li, X. Mi, Q. Luo, B. D. Hammock, C. Tan, Y. Chen and T. Pan, *Lab Chip*, 2019, **19**, 3405–3415.
- 22 M. Weiss, S. Gerber, R. M. Fuchslin and T. A. Neff, *Anaesthesia*, 2004, **59**, 1133–1137.
- 23 S. Gumbs, *Clin. J. Surg.*, 2019, **2**, 1–5.